

https://dspace.org/

The dynamics of mine hoist catenaries

Constancon, Charles Peter

2011-04-20
http://hdl.handle.net/10539/9610

Downloaded from a DSpace repository. https://dspace.org/

The catenary remains in contact with the sheave, admitting longitudinal motion tangential to the equilibrium profile ie. $\delta v(l_c) = 0, \delta w(l_c) = 0$. No slip occurs across the sheave; finally the lateral motion of the vertical rope is restrained.

The transport velocity of the rope is neglected with respect to longitudinal motion, but is included with respect to the lateral catenary motion[2].

5.1.2 Reduced Equations of Motion

Applying these simplifications, the undamped[3] nonlinear equations of motion of the mine hoist system are defined as.

$$(1 + \zeta\delta(s - l_c) + \eta\delta(s - l_v))u_{tt} = c^2 u_{ss} + c^2(v_s v_{ss} + w_s w_{ss} - \kappa v_s)[H(s) - H(s - l_c)] \tag{5.1}$$

Where $\zeta = \frac{I}{\rho A R^2}, \eta = \frac{M}{\rho A}$, and l_c, l_v refer to the length of the catenary and vertical rope respectively[4].

$$v_{tt} + 2Vv_{s,t} = (\bar{c}^2 - V^2)v_{ss} + c^2\left[v_s\{u_s - \kappa v + \tfrac{1}{2}(v_s^2 + w_s^2)\}\right]_s + \kappa\{u_s - \kappa v + \tfrac{1}{2}(v_s^2 + w_s^2)\} \tag{5.2}$$

$$w_{tt} + 2Vw_{s,t} = (\bar{c}^2 - V^2)w_{ss} + c^2\left[w_s\{u_s - \kappa v + \tfrac{1}{2}(v_s^2 + w_s^2)\}\right]_s \tag{5.3}$$

Where c^2, and $\bar{c}^2$ represent the longitudinal and lateral wave speeds, κ represents the catenary curvature, and V the axial transport velocity of the rope.

---

[2]This follows from the observation that the importance of the Coriolis coupling is dependent on the ratio of the transport velocity to the wave speed. ie $\frac{V}{\bar{c}} \approx 10^{-1}$, where as $\frac{V}{c} \approx 10^{-3}$, where $c, \bar{c}$ represent the longitudinal and lateral wave speed respectively.

[3]Since a proportional damping mechanism is applied, modal damping factors will be introduced at a later stage.

[4]I, R, M, E, A refer to the sheave inertia, sheave radius, conveyance mass, modulus of elasticity, and effective steel area of the rope respectively.

5.2 Normal Mode Model of the Equations of Motion

Initially the normal mode technique was applied to discretise the equations of motion. Although this technique is commonly applied to obtain approximate solutions to weakly nonlinear continuous systems, it was found that the simulation based on this method did not correlate with laboratory measurements. For this reason an alternative technique was ultimately applied. Nevertheless, the normal mode technique applied to model the system is presented and discussed for the purpose of documenting the limitations of this approach.

In applying the normal mode method, trivial boundary conditions are required, such that the spatial variables can be approximated by applying the linear eigenfunctions or normal modes of the system. This can be accomplished by transforming the equations of motion so that the boundary excitation is introduced as distributed inertial forces in the equations of motion.

The following transformation is a valid transformation[5].

$$u(s,t) = u(0,t) - \frac{1}{2l_c}[v(0,t)^2 + w(0,t)^2]\left\{\frac{s}{l_c}[H(s) - H(s-l_c)] + H(s-l_c)\right\} + \frac{\kappa}{2l_c}s(2l_c - s)[H(s) - H(s-l_c)]w(0,t) + \overline{u}(s,t)$$

$$v(s,t) = v(0,t)(1 - \frac{s}{l_c}) + \overline{v}(s,t)$$

$$w(s,t) = w(0,t)(1 - \frac{s}{l_c}) + \overline{w}(s,t)$$

Substituting these co-ordinate transformations into the equations of motion (5.1,5.3,5.2), leads to a set of equations, where the boundary excitation induces an equivalent distributed inertial load. In this reference frame, trivial

[5]This transformation ensures that the longitudinal strain remains unchanged during a static rigid body displacement, in accordance with the tension compensation mechanism induced by the sheave interface ie the equation of motion at the sheave due to a static displacement field reduces to $[u_s - \kappa v + \frac{1}{2}(v_s^2 + w_s^2)|_1 = u_s|_2 = 0$, where $1, 2$ refer to stations on the catenary and vertical sides of the sheave respectively. The transformation adopted satisfies this condition.

boundary conditions exist at the winder drum. Since the excitation in the in-plane direction $v(0,t)$ is of the order of 0.5mm, it is included only as a weak source of direct excitation of the in-plane motion. For this reason, it is not carried through the subsequent equations, and results only in defining the direct excitation of the in-plane motion $F_v(s,t)$.

$$\begin{aligned}(1+\zeta\delta(s-l_c)+\eta\delta(s-l_v))\overline{u}_{tt} &= c^2\overline{u}_{ss} \\ +c^2[\overline{v}_s\overline{v}_{ss}+\overline{w}_s w_{ss} &- \frac{1}{l_c}w(0,t)\overline{w}_{ss}-\kappa\overline{v}_s][H(s)-H(s-l_c)] \\ &+F_u(s,t)\end{aligned} \tag{5.4}$$

$$\begin{aligned}\overline{v}_{tt}+2V\overline{v}_{s,t} = \; & (c^2-V^2)\overline{v}_{ss}+c^2\left[(\overline{u}_s\overline{v}_s)_s+\tfrac{3}{2}(\overline{v}_s)^2\overline{v}_{ss}+\tfrac{1}{2}(\overline{w}_s^2\overline{v}_s)_s\right] \\ & -\kappa c^2\left[\overline{v}\;\overline{v}_{ss}-\overline{u}_s+\kappa\overline{v}-\tfrac{1}{2}(\overline{w}_s)^2+\tfrac{1}{2}(\overline{v}_s)^2\right] \\ & -c^2\tfrac{w(s,t)}{l_c}\left[(\overline{w}_s\overline{v}_s)_s+\kappa\overline{w}_s\right]+F_v(s,t)\end{aligned} \tag{5.5}$$

$$\begin{aligned}\overline{w}_{tt}+2V\overline{w}_{s,t} = \; & (c^2-V^2)\overline{w}_{ss}+c^2\left[(\overline{u}_s\overline{w}_s)_s+\tfrac{3}{2}(\overline{w}_s)^2\overline{w}_{ss}+\tfrac{1}{2}(\overline{v}_s^2\overline{w}_s)_s\right] \\ & -\kappa c^2\left[\overline{v}\;\overline{w}_{ss}+\overline{w}_s\overline{v}_s\right] \\ & c^2\tfrac{w(0,t)}{l_c}\left[\tfrac{w(0,t)}{l_c}\overline{w}_{ss}-\overline{v}_{ss}-3\overline{w}_s\overline{w}_{ss}-\overline{v}_s\overline{v}_{ss}+\kappa\overline{v}_s\right] \\ & +F_w(s,t)\end{aligned} \tag{5.6}$$

where:

$$\begin{aligned}F_u(s,t) = \; & -[1+\zeta\delta(s-l_c)+\eta\delta(s-l_v)]\times \\ & \left\{\tfrac{\partial^2 u(0,t)}{\partial t^2}-\tfrac{1}{2l_c}\tfrac{\partial^2[u(0,t)]^2}{\partial t^2}\right\}\left[[H(s)-H(s-l_c)]\tfrac{s}{l_c}+H(s-l_c)\right]\end{aligned}$$

$$F_v(s,t) = -(1-\frac{s}{l_c})\frac{\partial^2 v(0,t)}{\partial t^2}+\frac{2V}{l_c}\frac{\partial v(0,t)}{\partial t}$$

$$F_w(s,t) = -(1-\frac{s}{l_c})\frac{\partial^2 w(0,t)}{\partial t^2}+\frac{2V}{l_c}\frac{\partial w(0,t)}{\partial t}$$

$$\overline{v}(0,t)=\overline{w}(s,t)=\overline{w}(0,t)=0$$

$$\overline{v}(l_c,t) = \overline{w}(l_c,t) = 0$$

It is evident that these equations of motion contain spatially distributed forcing functions, as well as terms with periodic coefficients. It is convenient to transform the partial differential equations into a set of ordinary differential equations. Usually this is accomplished by means of the expansion theorem (Meirovitch[1970]), where the solution is expanded in terms of a superposition of the linear eigenfunctions (the normal modes) multiplied by time dependent functions. Since the dynamic characteristics of the mine hoist system are non-stationary due to the changing length of the vertical rope, this approach cannot be applied directly. The normal mode expansion may be applied to approximate the non-stationary spatial domain by assuming that the vertical length changes *slowly* with time. In this context, *slowly* means that small changes in the dynamic characteristics occur during a period of the fundamental frequency of the system. This condition applies to the mine hoist system except towards the shaft head, where the longitudinal system characteristics change significantly over a short depth. If the system is treated as one with *slowly varying* parameters, then the change in the vertical length l, which introduces the non-stationary nature to the spatial variables, can be observed on a *slow* time scale $\tau = \epsilon t$, where ϵ is a small parameter. In this case an approximate solution can be found by considering an expansion of the form, $\sum_{n=1}^{\infty} \phi(s,l)_n q_n(t)$, where $\phi_n(s,l)$ represents the eigenfunction of the nth mode, and $l = l(\tau)$. Thus the eigenfunctions can be found as a function of the vertical length $l(\tau)$, and applied to transform the system to ordinary differential form discreetly during the numerical simulation[6]. Since the boundary conditions applicable to the transformed partial differential equations of motion are trivial, a normal mode method is readily applied to convert the partial differential equations into nonlinear ordinary differential form ie.

$$\overline{u}(s,t) = \sum \phi(s)q(t)$$

$$\overline{v}(s,t) = \sum \Phi(s)p(t)$$

$$\overline{w}(s,t) = \sum \Phi(s)r(t)$$

[6]If one Accounts for the *slowly* varying properties of the dynamic characteristics, additional terms are introduced in the equations of motion. This effect is being considered by Kaczmarczyk[1993].

Substituting the normal mode expansions into equations (5.4,5.5,5.6), and orthogonalising these equations with respect to the linear normal modes ϕ_i, Φ_i, a set of nonlinear ordinary differential equations result[7].

$$\ddot{p}_i + 2\zeta_u\omega_i\dot{p}_i + \omega_i^2 p_i + (\frac{v(0,t)}{l_c})U_{ij}^u r_j + K_{ij}^u q_j + \Gamma_{ijk}[r_j r_k + q_j q_k] = P_i(t) \tag{5.7}$$

$$\begin{aligned} \ddot{q}_i + 2(\zeta_w\overline{\omega}_i + V\mathcal{V}_{ij})\dot{q}_i + \overline{\omega}_i^2 q_i &+ \Delta_{ijk}p_j q_k \\ +\beta_{ijkl}(\frac{3}{2}q_j q_k q_l + \frac{1}{2}r_j r_k q_l + r_j q_k r_l) &+ \gamma_{ijk}q_j q_k + \\ \epsilon_{ij}p_j + \eta_{ijk}(q_j q_k - r_j r_k) - \kappa K_{ij}q_j &+ \frac{v(0,t)}{l_c}(\zeta_{ijk}r_j q_k + K_{ij}^w r_j) = Q_i(t) \end{aligned} \tag{5.8}$$

$$\begin{aligned} \ddot{r}_i + 2(\zeta_v\overline{\omega}_i + V\mathcal{V}_{ij})\dot{r}_i + \overline{\omega}_i^2(1 + (\frac{c}{c_l})^2(\frac{v(0,t)}{l_c})^2)r_i &+ \Delta_{ijk}p_j r_k \\ +\beta_{ijkl}(\frac{3}{2}r_j r_k r_l + \frac{1}{2}q_j q_k r_l + q_j r_k q_l) &+ \alpha_{ijk}q_j r_k + \\ \frac{v(0,t)}{l_c}\left[U_{ij}^v p_j + \delta_{ijk}(3r_j r_k + q_j q_k) + K_{ij}q_j\right] &= R_i(t) \end{aligned} \tag{5.9}$$

Where:

$$\overline{\omega}_i^2 = [1 - (\frac{V}{c})^2]^{\frac{1}{2}}\frac{i\pi}{l_c}\overline{c}$$
$$K_{ij}^u = \frac{\kappa c^2}{m_{ii}^v}\int_0^{l_c}\phi_i(s)\Phi_j'(s)ds$$
$$\mathcal{V}_{ij} = \frac{1}{m_{ii}^v}\int_0^{l_c}\Phi_i(s)\Phi_j'(s)ds$$
$$\delta_{ijk} = \frac{c^2}{m_{ii}^v}\int_0^{l_c}\Phi_i(s)\Phi_j'(s)\Phi_k''(s)ds$$
$$U_{ij}^v = \frac{c^2}{m_{ii}^v}\int_0^{l_c}\Phi_i(s)\phi_j''(s)ds$$
$$K_{ij} = -\frac{\kappa c^2}{m_{ii}^v}\int_0^{l_c}\Phi_i(s)\Phi_j(s)ds$$
$$\epsilon_{ij} = -\frac{\kappa c^2}{m_{ii}^v}\int_0^{l_c}\Phi_i(s)\phi_j'(s)ds$$
$$K_{ij}^w = \frac{\kappa c^2}{m_{ii}^v}\int_0^{l_c}\Phi_i(s)\Phi_j'(s)ds$$
$$m_{ii}^v = m_{ii}^w = \int_0^{l_c}[\Phi_i(s)]^2 ds$$
$$P_i(t) = \frac{1}{m_{ii}^v}\int_0^{l_v}F_u(s,t)ds$$
$$R_i(t) = \frac{1}{m_{ii}^w}\int_0^{l_v}F_w(s,t)ds$$

$$U_{ij}^u = \frac{c^2}{m_{ii}^v}\left\{\int_0^{l_c}\phi_i(s)\Phi_j''(s)ds - \phi_i(l_c)\Phi_j'(l_c)\right\}$$
$$\Gamma_{ijk} = -\frac{c^2}{m_{ii}^v}\left\{\int_0^{l_c}\phi_i(s)\Phi_j'(s)\Phi_k''(s)ds - \frac{1}{2}\phi_i(l_c)\Phi_j'(l_c)\Phi_k'(l_c)\right\}$$
$$\Delta_{ijk} = -\frac{c^2}{m_{ii}^v}\int_0^{l_c}\Phi_i(s)\{\phi_j''(s)\Phi_k'(s) + \phi_j'(s)\Phi_k''(s)\}ds$$
$$\beta_{ijkl} = -\frac{c^2}{m_{ii}^v}\int_0^{l_c}\Phi_i(s)\Phi_j'(s)\Phi_k'(s)\Phi_l''(s)ds$$
$$\alpha_{ijk} = \frac{\kappa c^2}{m_{ii}^v}\int_0^{l_c}\Phi_i(s)\{\Phi_j(s)\Phi_k''(s) + \Phi_j'(s)\Phi_k'(s)\}ds$$
$$\gamma_{ijk} = \frac{\kappa c^2}{m_{ii}^v}\int_0^{l_c}\Phi_i(s)\Phi_j(s)\Phi_k''(s)ds$$
$$\eta_{ijk} = \frac{\kappa c^2}{2m_{ii}^v}\int_0^{l_c}\Phi_i(s)\Phi_j'(s)\Phi_k'(s)ds$$
$$\zeta_{ijk} = \frac{c^2}{m_{ii}^v}\int_0^{l_c}\Phi_i(s)\{\Phi_j'(s)\Phi_k''(s) + \Phi_j''(s)\Phi_k'(s)\}ds$$
$$m_{ii}^u = \int_0^{l_c+l_v}[\phi_i(s)]^2 ds + \zeta[\phi(l_c)]^2 + \eta[\phi(l_v)]^2$$
$$Q_i(t) = \frac{1}{m_{ii}^v}\int_0^{l_v}F_v(s,t)ds$$

[7]Modal damping is added to the equation of motion via $\zeta_{u,v,w}$.; where ζ may be defined to account for a general proportional viscous damping mechanism as defined in Appendix G

During the accelerating or decelerating phase of the winding cycle, or at layer change where the rope rises in the in-plane direction by a full rope diameter, transient excitation is applied to the system. This excitation can be accounted for in the equations of motion by introducing additional inertial forces. At a layer change, the reversal in the direction of traverse in the out-of-plane direction can be accounted for by changing the phase of the out-of-plane excitation appropriately. Thus the ordinary differential equations of motion of the mine hoist system are expressed in a concise form, and readily coded in a numerical simulation. Initial simulation trials provided convincing results. In fact the simulation of the Kloof mine hoist system based on the normal mode model correlated well with the observations of Dimitriou and Whillier[1973]. Such a simulation is presented in figure 5.1, for the ascending and descending cycle of the Kloof Hoist system, between the depths of 50-1400 m[8]. In this figure, the in and out-of-plane lateral motion at the quarter point of the catenary, and the longitudinal motion of the sheave and skip are presented. Large lateral catenary motion is evident on the ascending cycle, as well as significant longitudinal oscillation at the sheave. The tension ratio across the sheave is sufficiently high on the ascending cycle, such that frictional slip across the sheave must occur. Such a condition invalidates the simulation, and the simulation was stopped short of the full wind. It is clear from this simulation that significant dynamic effects could be expected on the ascending cycle, as confirmed by Dimitriou and Whillier's observations. The acceleration and deceleration phase of the winding cycle, as well as the transient response induced by a layer change over is clearly marked. Layer change over locations are represented by the vertical lines in the figure. The in-plane motion is referenced to the chord line between the drum and sheave, and consequently the mean position rises with increasing shaft depth in accordance with the decreasing rope curvature due to the increasing vertical rope mass and thus catenary tension.

[8]The Kloof Mine hoist system actually extends over a 2100m shaft depth. The simulation was executed over a 1400m shaft depth to emulate Mankowski's simulation. It is not clear why Mankowski truncated the shaft depth in his simulation; it is presumed that this was to reduce the simulation time.

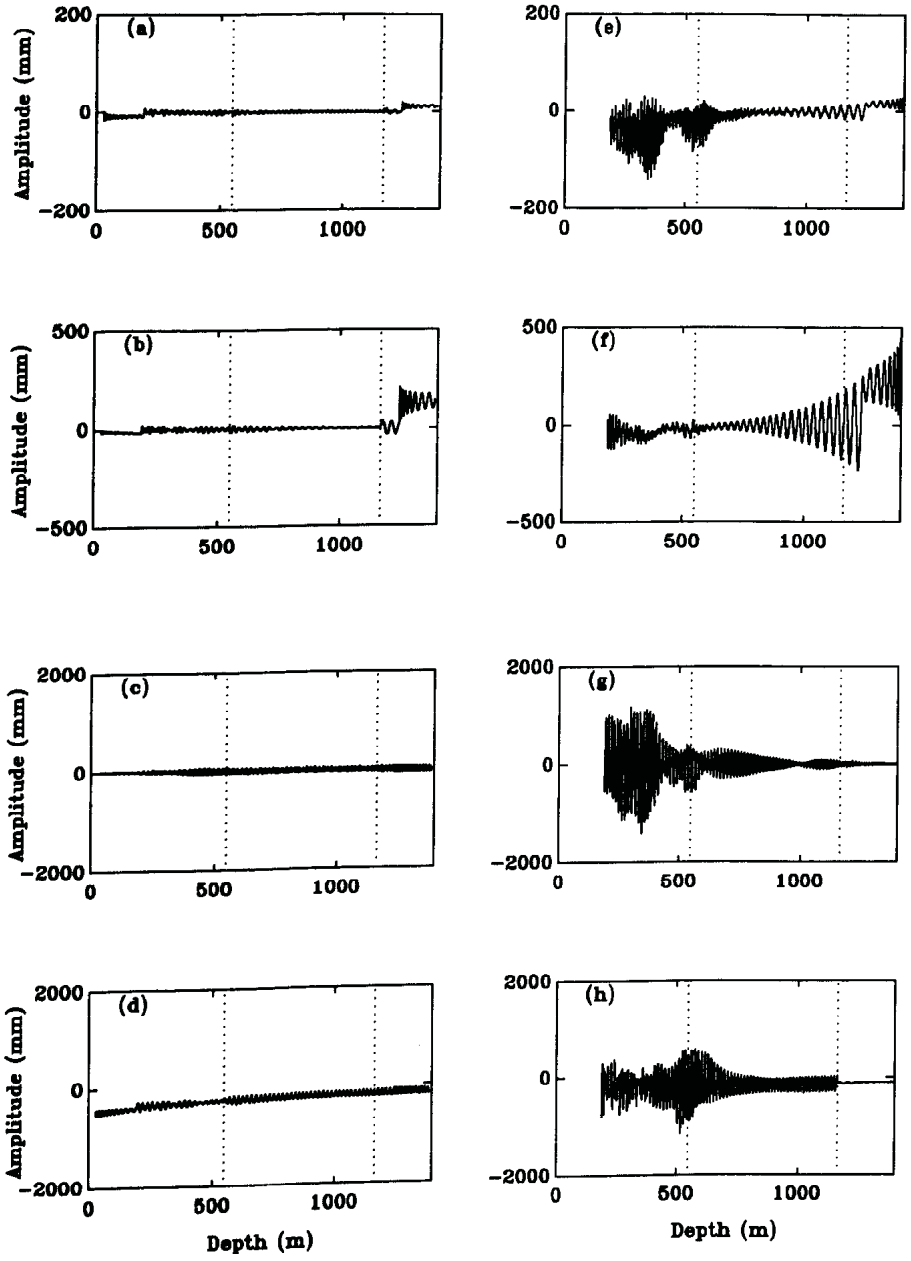

Figure 5.1: Kloof Mine simulation - Normal mode model

(a-d) - Descending Wind.
(a,e) Sheave Displacement.
(c,g) Out-of-plane Lateral Motion - $s = l_c/4$
(e-h) - Ascending Wind.
(b,f) Skip Displacement.
(d,h) In-plane Lateral Motion - $s = l_c/4$

Reservations concerning the applicability of the normal mode method with reference to nonlinear dynamic systems, lead to an examination of the degree of correlation attainable between numerical results, and experimentally extracted measurements. Since an accurate correlation exercise from on site measurements would be difficult to control, the stationary laboratory model was applied. It was clear that although the numerical simulation correctly predicted the onset of in-plane motion, the amplitudes were grossly incorrect within regions of primary and secondary resonance. It is noted that in the laboratory experiment, sinusoidal excitation amplitudes of 1mm were applied for a 475mm catenary length. In the context of the mine hoist system, excitation amplitudes of 7mm are applied to catenary lengths of 70m. Clearly the level of excitation applied in the laboratory experiment was significantly higher; perhaps it could be argued that for lower levels of excitation the system would be weakly nonlinear and hence the normal mode method would be appropriate. Since the transient excitations applied to the mine hoist system during layer changes, and during the acceleration/deceleration profiles are significant, it was decided not to accept the normal mode method. On comparing the numerical results to experimental measurements, it was evident that the numerical simulation predicted substantial stiffening, resulting in a pronounced backbone, whereas the experimental measurements indicated that the laboratory model did not exhibit a backbone.

In applying the normal mode method, it is assumed that the linear normal modes of the system form a spatial basis for the nonlinear motion. This assumption has found acceptance on condition that the system conforms to that of a weakly nonlinear system, where the nonlinear motion remains close to that of the linear motion. Szemplinska-Stupnika [1983] considered the validity of such an assumption, and proposed the nonlinear normal mode method. In this approach, Szemplinska-Stupnika calculated the nonlinear steady state response of a system via the conventional normal mode method, and the nonlinear normal mode method proposed. Since the steady state response was considered, a harmonic temporal response was assumed, and the equations of motion resulted in nonlinear ordinary differential equations describing the spatial domain and boundary conditions of the solution. Significant differences in the response were found. Nayfeh et al[1992] considered this problem, with reference to continuous systems with quadratic and cubic nonlinearities. Nayfeh et al. applied perturbation techniques directly to the Lagrangian of the system, followed by averaging over the fast time scale to obtain the ordinary differential equations that govern the modulation and phase of the response directly. Nayfeh et. al observed that the conventional normal mode technique is based on applying a Galerkin procedure to minimise errors between the assumed and exact spatial distribution, leading to ordinary nonlinear differential equations of motion which minimise this error. By considering a simple non-

linear system with quadratic and cubic nonlinearities for various conditions of tuning, Nayfeh et al. demonstrated that the normal mode technique generally fails to correctly account for the spatial variations of the drift terms, and other harmonics. It also incorrectly predicts the effective nonlinearity and the nonlinear frequency shift.

At the stage of completing the laboratory experiment, a significant effort had been invested in developing the normal mode simulation of the mine hoist system. The significance of the effect of the normal mode approximation on the response was not fully appreciated. Although it would be expected that a simulation model based on a normal mode approach would exhibit modal truncation, it was not expected that the truncation would be so severe that it would drastically alter the dynamic characteristics of the system. In an attempt to investigate the aspect of modal truncation, additional longitudinal modes were included with little success. It became evident that the normal modes related to the linear eigenfunctions of the longitudinal system, could not adequately describe the tension distribution in the catenary, as induced by the lateral motion; in particular the drift term in the longitudinal equation of motion which is produced by the quadratic coupling of the longitudinal co-ordinate to the lateral motion was not correctly accounted for, as supported by Nayfeh et al. This feature of the normal mode model occurs as a result of applying the linear eigenfunctions to the spatial domain, which are not compatible with the nonlinear deformation relationship in the catenary. Thus constraint forces are induced in the system, and the tension compensation normally afforded by the sheave interface is disrupted. As a result the nonlinear nature of the system is aliased by the presumed dynamic motion.

If one considers a quasi-static relationship for the catenary then a constraint equation develops relating the longitudinal to lateral motion, such that the quasi-static strain in the catenary is described by: $g(t) = u_s + \frac{1}{2}(v_s^2 + w_s^2)$. In applying a normal mode method, it is assumed that the lateral motion $v(s) = \Phi(s)q(t), w(s) = \Phi(s)r(t)$, where $\Phi(s) = sin(\frac{\pi s}{l_c})$; as a result, a quasi-static deformation would require that the longitudinal deformation in the catenary permits a longitudinal strain deformation of the form $u_s = g(t)+A+Bcos(\frac{2\pi s}{l_c})$. If a normal mode based on the continuous longitudinal system is applied, such a relationship cannot be accommodated. Furthermore, longitudinal modes with a wavelength of the order of the catenary section would imply short wavelengths in the vertical section. As a result, although the spatial distribution $Bcos(\frac{2\pi s}{l_c})$, may be satisfied in the catenary section by the inclusion of higher longitudinal modes, the normal co-ordinates involved would require elastic deformation of the vertical section, and thus constrain the longitudinal motion. This problem can be overcome by splitting the system at the sheave, and applying fixed free normal modes to the catenary section alone.

The catenary section could then be coupled to the sheave and vertical longitudinal system with independent normal co-ordinates. Thus the vertical system would contain a rigid body mode, enabling the tension to be correctly distributed between the catenary and vertical section. Considering the mine rope system, the catenary is generally shorter than the vertical system, and the natural frequencies of the normal co-ordinates applied to model the catenary section would be significantly higher than the response and excitation frequencies. As a result the retention of longitudinal inertia in the catenary section is unnecessary. A more usual proposition supporting this notion is that since the longitudinal wave speed in the catenary section is far greater than the lateral wave speed, the interaction between longitudinal and lateral motion would occur in a quasi-static manner, where the tension distribution in the catenary is spatially uniform. Since the retention of longitudinal inertia in the catenary section is thus unlikely to be significant, and would increase the number of co-ordinates required in the simulation model, it is sensible to apply a quasi-static description to the catenary section directly. The implication of a quasi-static constraint is that secondary regions of resonance related to combination parametric resonance involving different lateral modes of the catenary would be eliminated (Perkins[1992b]). However, on the basis of the stability chart extracted from the laboratory experiment, such regions are less significant and more difficult to excite. The more important combination resonance involving the lateral and longitudinal system would be accounted for due to the retention of the longitudinal inertia of the vertical section. This observation prompted a reappraisal of the normal mode discretisation technique, leading to the development of a more conventional quasi-static model of the mine hoist system.

5.3 Laboratory Measurements

A validation of the the numerical simulation was achieved by considering the laboratory model introduced in chapter 4. The laboratory model was tuned to the first case presented in tables (4.1),(4.2) of chapter 4. The system was excited with a constant amplitude, and the envelope of the motion in the in and out-of-plane direction, at the mid point of the string was measured visually. It would have been useful to track the motion of the guitar string, so that polar plots of the steady state motion could be directly compared with the results of the numerical simulation, however suitable measurement transducers were not available. The envelope of the motion was measured with video CCD cameras. A camera was aligned normal to each plane. A screen lined with graph paper was placed behind the guitar string, within the focal depth of the camera, such that the envelope of the steady state motion could be detected visually. The excitation frequency was increased incrementally, and the amplitude of the excitation was adjusted so that it remained constant. This process was repeated for excitation amplitudes of 0.1,0.5 and 1mm, over a bandwidth from 40-80 Hz. The measurement resolution was judged to be of the order of 0.5 mm.

The experimental envelope of the in and out-of-plane motion is presented in figure 5.2 for three sinusoidal excitation amplitudes of 0.1, 0.5 and 1 mm. This figure reflects the in and out-of-plane motion simultaneously, where the positive absolute motion of the out-of-plane and the negative absolute motion of the in-plane response is presented on a single axis. During the experiment, it was found that non-planar motion developed rapidly. It also became evident that the system did not exhibit a *backbone*, and consequently non-planar motion developed at approximately the same frequency regardless of whether the the excitation frequency was increased or decreased. An interesting region of motion was observed between approximately 55-57 Hz, where large non-planar motion occurred. The motion was clearly non-periodic, and it was not possible to measure the amplitude of the envelope consistently by using the video camera technique. A beating motion appeared to develop between the in and out-of-plane modes, and the motion appeared to be chaotic. Whereas the region close to primary resonance at 53 Hz resulted in the mass being raised to a new equilibrium level due to the arc length change in the catenary, the region between 54-57 Hz was characterised by substantial longitudinal dynamic motion, and a saturation phenomenon appeared to develop with respect to the lateral modes.

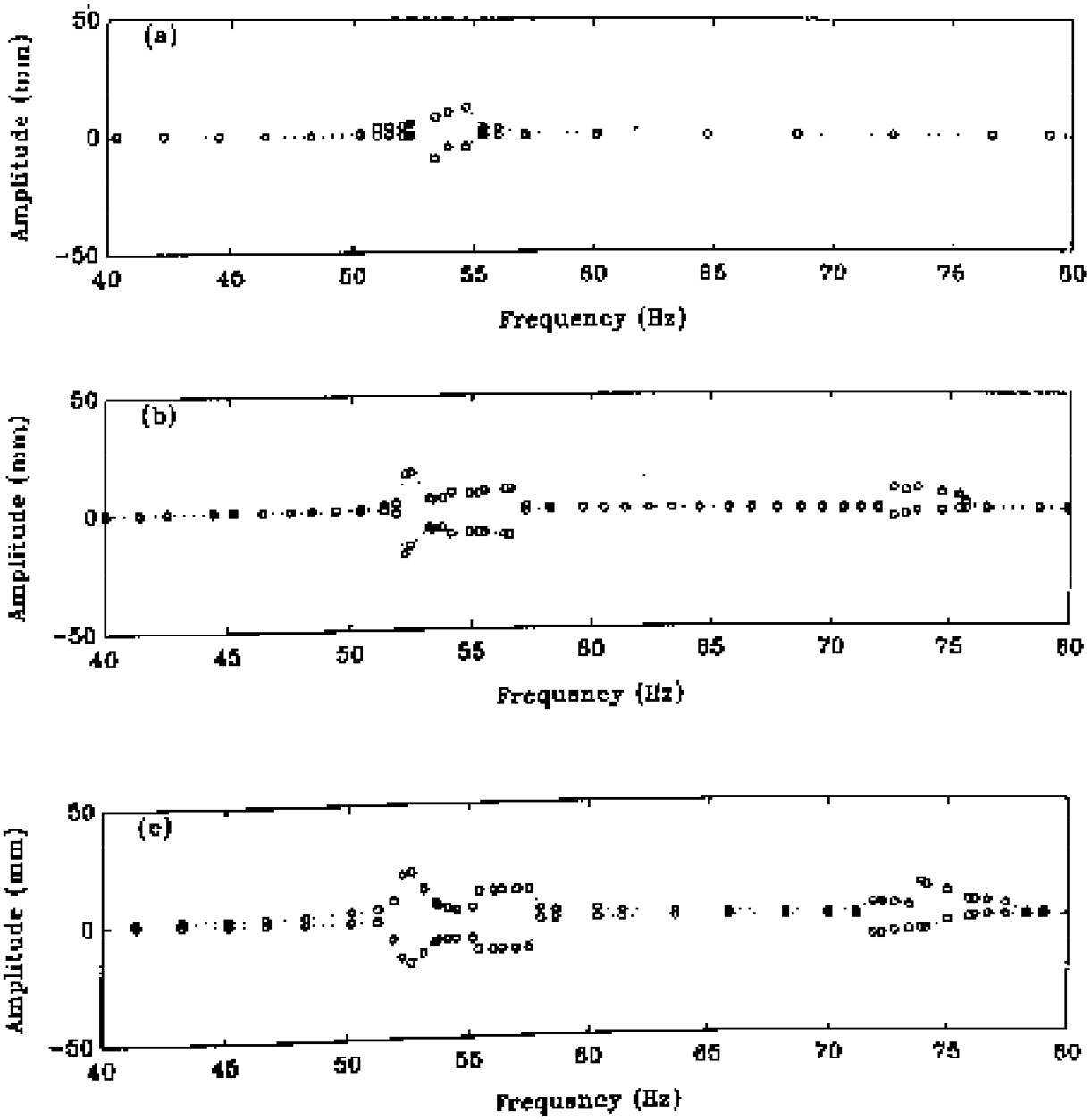

Figure 5.2: Experimental steady state amplitudes

(a) 0.1 mm Excitation amplitude.
(b) 0.5 mm Excitation amplitude.
(c) 1 mm Excitation amplitude.

5.4 Quasi-Static Laboratory Model

A quasi-static model is developed by considering the catenary and vertical section separately and imposing equilibrium and compatibility at the sheave. In the laboratory model, the pulley wheel is light, and is neglected. A schematic of the laboratory model is presented in figure 5.3.

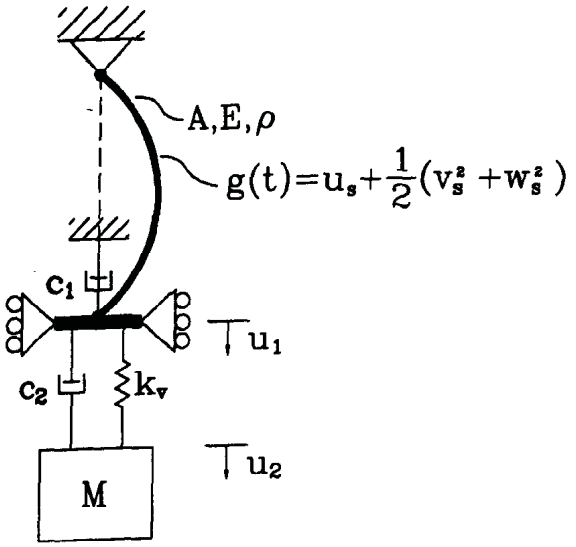

Figure 5.3: Quasi-static laboratory model

The equations of motion of the catenary section are:

$$u_{tt} = c^2[u_s + \frac{1}{2}(v_s^2 + w_s^2]_s \tag{5.10}$$

$$v_{tt} = \bar{c}^2 v_{ss} + c^2 \left\{[u_s + \frac{1}{2}\{(v_s)^2 + (w_s)^2\}]v_s\right\}_s \tag{5.11}$$

$$w_{tt} = \bar{c}^2 w_{ss} + c^2 \left\{[u_s + \frac{1}{2}\{(v_s)^2 + (w_s)^2\}]w_s\right\}_s \tag{5.12}$$

By neglecting the longitudinal inertia in equation (5.10), a quasi-static constraint relationship develops whereby:

$$u_s + \frac{1}{2}(v_s^2 + w_s^2) = g(t)$$

$g(t)$ represents the quasi-static strain in the catenary which is spatially uniform. This constraint relationship enables u_s to be formulated as:

$$u_s = g(t) - \frac{1}{2}(v_s^2 + w_s^2) \tag{5.13}$$

Substituting the quasi-static relationship into equations (5.11,5.12) results in the quasi-static description of the lateral equations of motion as:

$$v_{tt} = \bar{c}^2\{1 + (\frac{c}{\bar{c}})^2 g(t)\}v_{ss} \tag{5.14}$$

$$w_{tt} = \bar{c}^2\{1 + (\frac{c}{\bar{c}})^2 g(t)\}w_{ss} \tag{5.15}$$

The quasi-static strain in the catenary can be evaluated by considering the equilibrium of the oscillator which is coupled to the catenary section. With reference to figure 5.3, these equations are developed as:

$$c_1\dot{u}_1 + c_2(\dot{u}_1 - \dot{u}_2) + k(u_1 - u_2) = -AEg(t)$$

$$M\ddot{u}_2 + c_2\dot{u}_2 + ku_2 = ku_1 + c_2\dot{u}_1$$

$$M\ddot{u}_2 = -AEg(t) - c_1\dot{u}_1$$

$$u_1 = g(t)l_c - y_a$$

$$y_a = \frac{1}{2}\int_0^{l_c}(v_s^2 + w_s^2)ds$$

Manipulating these equations, the equation of motion for the suspended mass is obtained as:

$$M[1 + \frac{k_c}{k}]\ddot{u}_2 + c_2\frac{k_c}{k}\dot{u}_2 + k_c u_2 = (c_2\frac{k_c}{k} - c_1)\dot{u}_1 - k_c y_a$$

where $k_c = \frac{AE}{l_c}$, which represents the static stiffness of the catenary section. Thus the equation can be written in standard form as:

$$\ddot{u}_2 + 2\zeta\omega_n\dot{u}_2 + \omega_n^2 u_2 = -\omega_n^2 y_a + \chi\dot{u}_1$$

where $\chi = 2\zeta\omega_n - c_1\frac{\omega_n^2}{k_c}$, and ω_n represents the natural frequency of the longitudinal system.

Since $\dot{u}_1 = \dot{g}(t)l_c - \dot{y}_a$ this equation reduces to:

$$\ddot{u}_2 + 2\zeta\omega_n\dot{u}_2 + \omega_n^2 u_2 = -\omega_n^2 y_a - \chi\dot{y}_a + \chi\dot{g}(t)l_c \tag{5.16}$$

The equation describing $g(t)$ is generated through further manipulation of the previous equations:

$$\dot{g}(t) = \frac{1}{l_c}(\dot{u}_1 + \dot{y}_a)$$

$$\dot{u}_1 = -\frac{AE}{c_1}g(t) - \frac{M}{c_1}\ddot{u}_2$$

This leads to:

$$\dot{g}(t) + \frac{k_c}{c_1}g(t) = -\frac{M}{c_1 l_c}\ddot{u}_2 + \frac{1}{l_c}\dot{y}_a \tag{5.17}$$

The lateral excitation at the slider is introduced by transforming the lateral coordinates such that the boundary conditions become trivial, and the dynamic motion is then referenced to the base motion. This is achieved by applying the transformation:

$$v(s,t) = \overline{v}(s,t) + \frac{v_o}{l_c}(1 - \frac{s}{l_c})$$

Introducing this transformation into equations (5.14,5.15,5.16,5.17) results in the forced equations of motion as:

$$\overline{v}_{tt} = \overline{c}^2\{1 + (\frac{c}{\overline{c}})^2 g(t)\}\overline{v}_{ss} + \frac{d^2}{dt^2}[(1 - \frac{s}{l_c})v_o] \tag{5.18}$$

$$\overline{w}_{tt} = \overline{c}^2\{1 + (\frac{c}{\overline{c}})^2 g(t)\}\overline{w}_{ss} \tag{5.19}$$

$$\ddot{u}_2 + 2\zeta\omega_n\dot{u}_2 + \omega_n^2 u_2 = -\omega_n^2\{y_a + (\frac{v_o^2}{2l_c})\}, \\ -\chi\{\dot{y}_a + \frac{d}{dt}(\frac{v_o^2}{2l_c}) - \dot{g}(t)l_c\} \tag{5.20}$$

$$\dot{g}(t) + \frac{k_c}{c_1}g(t) = -\frac{M}{c_1 l_c}\ddot{u}_2 + \frac{1}{l_c}\dot{y}_a + \frac{1}{l_c}\frac{d}{dt}(\frac{v_o^2}{2l_c}) \tag{5.21}$$

Examining these equations, it is evident that if the average damping effort in the catenary section is equivalent to that in the suspended oscillator, then $\chi = 0$. Additional concentrated damping at the sheave can be accommodated by making $\chi < 0$. Since the longitudinal equation and that for the quasi-static strain are coupled, they may be further reduced to produce a single third order ordinary differential equation of motion for the suspended system.

The equation of motion for the suspended mass, and that for the quasi-static strain $g(t)$ are ordinary differential equations. The equations of motion for the lateral motion of the catenary are converted to ordinary differential form by applying a normal mode expansion:

$$v(s,t) = \sum \Phi_i(s)q_t$$

$$w(s,t) = \sum \Phi_i(s)r_t$$

Applying this expansion to equations (5.18,5.19), and orthogonalising the equations in the usual manner, a set of nonlinear ordinary differential equations result. For the special case where the longitudinal damping ζ, C_1 is zero, the equations can be represented as a set of coupled nonlinear ordinary differential equations, with quadratic and cubic nonlinearities. In the absence of longitudinal damping, the longitudinal equation of motion can be incorporated into the equation describing the quasi-static strain $g(t)$ to give:

$$g(t) = \omega_n^2\frac{M}{AE}\{u_2 + y_a + (\frac{v_o^2}{2l_c})\}$$

Applying the normal mode expansion for the lateral motion $v(s,t), w(s,t)$:

$$y_a = \alpha_i\{q_i^2 + r_i^2\}$$

Thus $g(t)$ can be written as:

$$g(t) = \gamma u_2 + \gamma \sum_{i=1}^{n} \alpha_i\{q_i^2 + r_i^2\} + \gamma(\frac{v_o^2}{2l_c})$$

where $\gamma = \frac{\omega_n^2 M}{AE}$. Applying the normal mode expansion to the lateral equations of motion, the equations of motion of the system are:

$$\ddot{q}_i + \omega_i^2 q_i + \beta(t)q_i + \Lambda_i q_i u_2 + \Gamma_{ij}\{q_i^2 + r_i^2\}q_j = F_q(t)$$

$$\ddot{r}_i + \omega_i^2 r_i + \beta(t)r_i + \Lambda_i r_i u_2 + \Gamma_{ij}\{q_i^2 + r_i^2\}r_j = 0$$

$$\ddot{u}_2 + \omega_n^2 u_2 + \omega_n^2 \alpha_i\{q_i^2 + r_i^2\} = -\omega_n^2(\frac{v_o^2}{2l_c})$$

where $\Gamma_{ij} = (\frac{c\omega_i}{\bar{c}})^2\alpha_i\gamma$, $\alpha_i = \frac{i^2\pi^2}{4l_c}$, $\Lambda_i = (\frac{c\omega_i}{\bar{c}})^2\gamma$,$\beta_i(t) = \gamma(\frac{c\omega_i}{\bar{c}})^2(\frac{v_o^2}{2l_c})$

It is apparent from these equations of motion, that the longitudinal system is quadratically coupled to the lateral modes. The lateral modes are quadratically coupled to the longitudinal mode, and cubic coupling arises due to the intermodal coupling of the lateral in and out-of-plane modes. In addition, the lateral system is subject to both parametric and external excitation, whilst the longitudinal system is subjected to external excitation only. Nayfeh and Mook[1983] discuss the analysis of ship pitch-roll motion with regard to a two degree of freedom model with quadratic nonlinearities. In the absence of parametric excitation ($\beta_i(t) = 0$) and cubic nonlinearity ($\Gamma_{ij} = 0$), the out-of-plane and longitudinal equations of motion for the laboratory model are similar in form to those analysed by Nayfeh and Mook, which are considered further in Appendix J.

5.4.1 Experimental Correlation

The quasi-static equations of motion developed for the laboratory model were coded with the Matlab-Simulink software programme. An Adams-Gear algorithm was applied with a variable step size and a relative integration error tolerance of 10^{-6}. The numerical simulation accounted for a single longitudinal mode, and two lateral modes in the in and out-of-plane directions. The physical parameters applied in the numerical simulation are tabulated in table 4.1 of chapter 4. It was assumed that the average longitudinal damping effort was equivalent in the catenary and vertical section of the string, and thus χ was set to zero.

For the purpose of the correlation, the numerical simulation was conducted at a series of points in 40-80 Hz range. Each simulation was executed for 40 seconds to allow the steady state motion to evolve. The comparison of the numerically simulated steady state response and the experimental results for an excitation amplitude of 0.5 mm is presented in figure 5.4.

It is evident that excellent correlation was achieved. It is interesting to observe that the plateaux region between 54-56 Hz is not related to the presence of the second lateral mode. In fact similar results are obtained for a single mode model. The plateaux region dissipates as the excitation amplitude reduces; it is characterised by strong longitudinal dynamic motion. An intensive study of the equations of motion would be required to adequately explain the observed behaviour. However, it is sufficient to observe that the equations of motion reflect quadratic coupling between the lateral and longitudinal mode, whilst quadratic and cubic coupling arises in the lateral equations of motion. The observed behaviour is attributed to the accentuated quadratic nature of the system due to the specific physical parameters, and consequently the plateaux region is characterised by a saturation phenomenon where the longitudinal dynamic motion develops at the expense of a saturated lateral motion. A secondary region of resonance occurs between 72-75 Hz. This region is related to the combination resonance of the longitudinal and first lateral mode. Although the out-of-plane measurements correlate well with the experimental measurements, larger in-plane motion is predicted by the simulation, resulting in a symmetrical response envelope. This is partly attributed to the neglect of gravity on the in-plane motion[9], but more likely due to differing boundary conditions in the two planes due to the physical construction of the model.

[9]Accounting for curvature in the in-plane mode introduces direct excitation of the symmetric in-plane modes. Although the curvature is small, a simulation which accounted for curvature of the string illustrated that the response envelope became asymmetrical, where the in-plane motion was ± 2mm less than the out-of-plane motion.

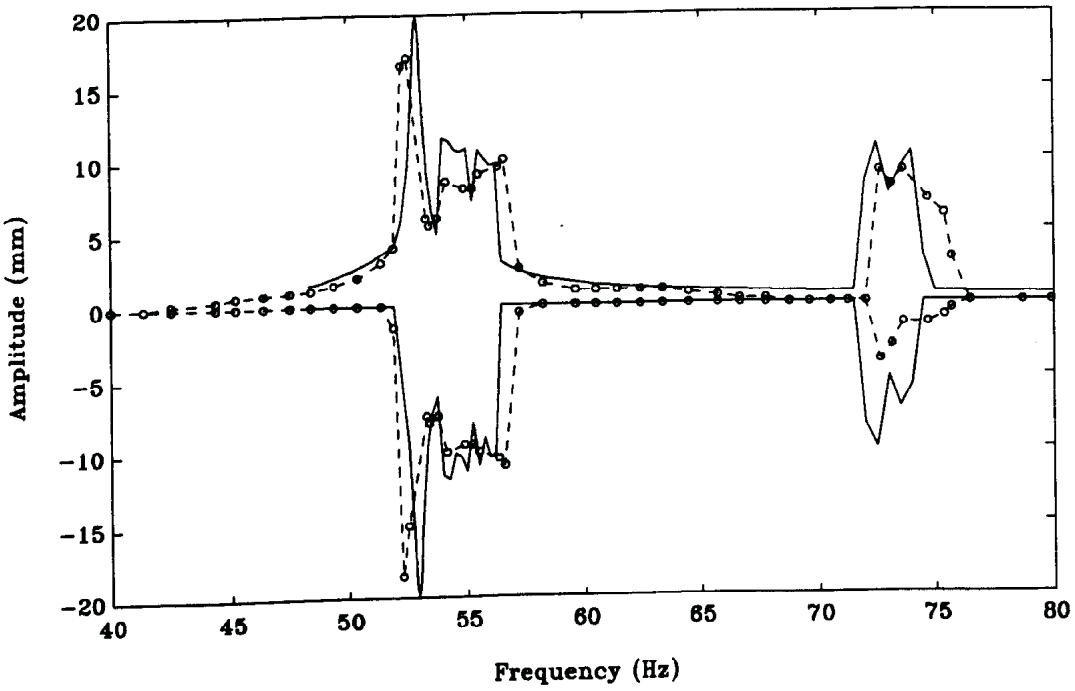

Figure 5.4: Experimental measurements vs simulation results

Steady state mid-plane response amplitudes.
- 0.5 mm excitation, two lateral in and out-of-plane modes.
_ _ o _ _ Experimental Measurements. —— Numerical Simulation.

Since the numerical simulation provided satisfactory correlation, the influence of non-stationary system parameters was examined. In the mine hoist system the vertical length of rope changes continuously during the wind, whilst the Lebus excitation frequency remains constant. Although the laboratory model was not necessarily scaled to parameters representative of the mine hoist system, it was decided to numerically assess the influence of a swept sine excitation on the response. Unfortunately measurements could not be made to confirm the numerically simulated results, nevertheless the numerical response presents interesting features. A sinusoidal sweep was applied to the numerical model between 40-60 Hz, and 60-80 Hz with a positive and negative sweep rate of 0.1 Hz/sec. A linear system subjected to a swept sinusoidal excitation reflects a delay in resonance with respect to the location of the steady state resonance. A study by Nayfeh and Asfar[1988], and Neal and Nayfeh[1990] on the non-stationary principal parametric excitation of a cubically nonlinear system demonstrates the passage through resonance for positive and negative sweep rates, illustrating the phenomena of penetration, overshoot and lingering or dragout of the response. Penetration refers to the phenomenon where the trivial response grows only after penetration of the region where the stationary trivial response is unstable; this is followed by an overshoot of the stationary non-trivial response and then convergence with the stationary non-trivial response. Lingering or dragout occurs for negative sweep rates, where the non-stationary response separates from the stationary response after convergence with it, and remains non-trivial after the stationary response is trivial. Surprisingly, in the numerical simulation of the laboratory model, the maximum response occurs as a precursor to the steady state resonance regardless of the direction of the sweep. Figures 5.5,5.6 present the response amplitudes for a positive and negative sweep rate at a 0.5mm excitation amplitude. An appreciable shift in the resonant peak with respect to the steady state response is observed. In addition response develops in regions where the steady state motion is small. A detailed explanation for this behaviour is not ventured. However, it is suggested that this behaviour is a result of the influence of the longitudinal system response on the lateral motion. In the case of the positive sweep rate, as the system approaches resonance, the suspended mass is drawn into the catenary, softening the system[10]. Since steady state motion is never attained, the lateral natural frequency drops promoting further growth. This causes the resonance to occur as a precursor to the steady state resonance. With regard to a negative sweep rate, the phase between the lateral and longitudinal motion is such that the average catenary tension rises due to the acceleration of the suspended mass, raising the catenary tension and once again promoting resonance as a precursor to the steady state resonant location. An explanation for the splitting of the resonance for a negative

[10]Such response was observed in the steady state simulations, where an overshoot in the longitudinal motion occurred prior to the system settling at a steady state amplitude.

sweep rate is not ventured. Clearly this system exhibits peculiar behaviour, and requires experimental and analytical validation in order to consistently explain the observed phenomena. This behaviour may have implications in the context of the mine hoist system, however, the excitation amplitudes and sweep rates are significantly less on the mine hoist system, and without an in-depth analytical study erroneous conclusions may be drawn. Finally, since the system inherently contains both quadratic and cubic coupling terms, it may be expected that the specific system parameters may influence the degree of quadratic and cubic coupling, and thereby the character of the response envelope significantly.

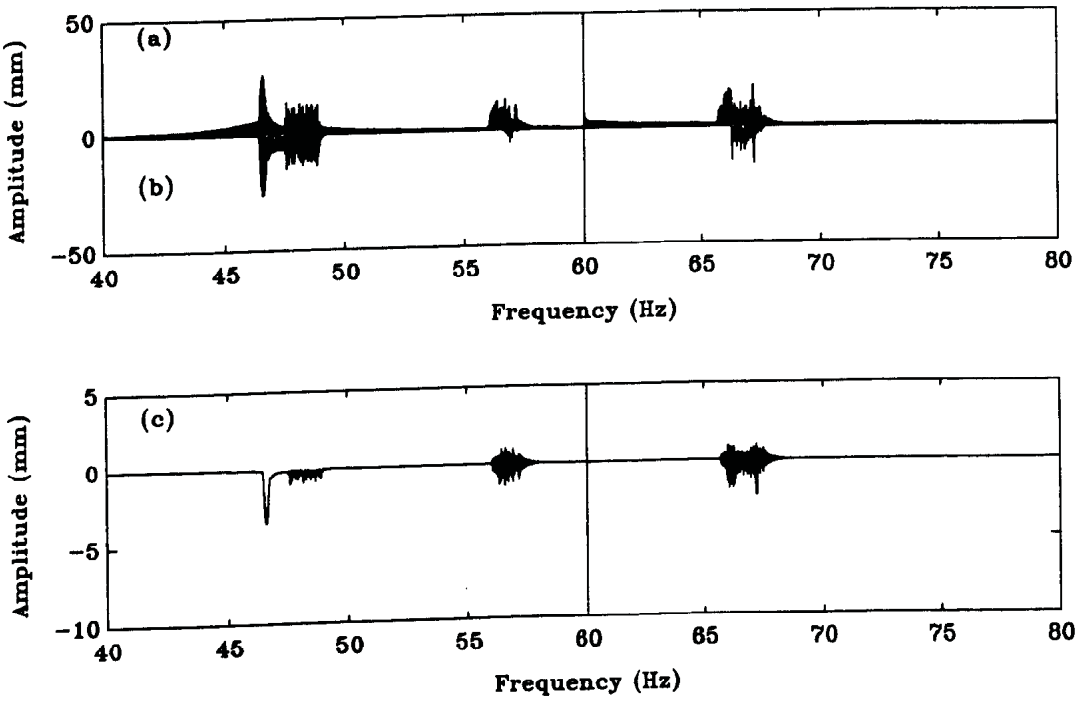

Figure 5.5: Sine sweep simulation - positive sweep rate.

Steady state mid-plane response amplitudes.
- 0.5 mm excitation, two lateral in and out-of-plane modes, 0.1 Hz/sec sweep rate.
(a) Out-of-plane Response.
(b) In-plane Response.
(c) Longitudinal response.

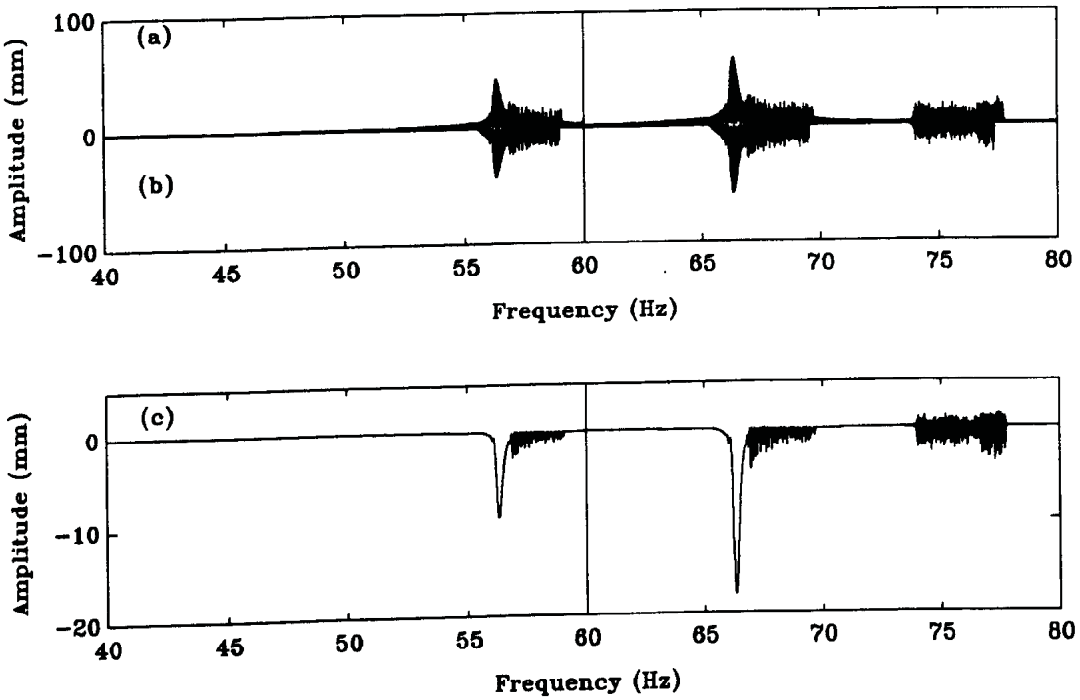

Figure 5.6: Sine sweep simulation - negative sweep rate.

Steady state mid-plane response amplitudes.
- 0.5 mm excitation, two lateral in and out-of-plane modes, -0.1 Hz/sec sweep rate.
(a) Out-of-plane Response.
(b) In-plane Response.
(c) Longitudinal response.

5.5 Quasi-Static Mine Hoist Model

A quasi static version of the mine hoist system was developed by following a similar procedure to that implemented for the laboratory model. This model is illustrated in figure 5.7.

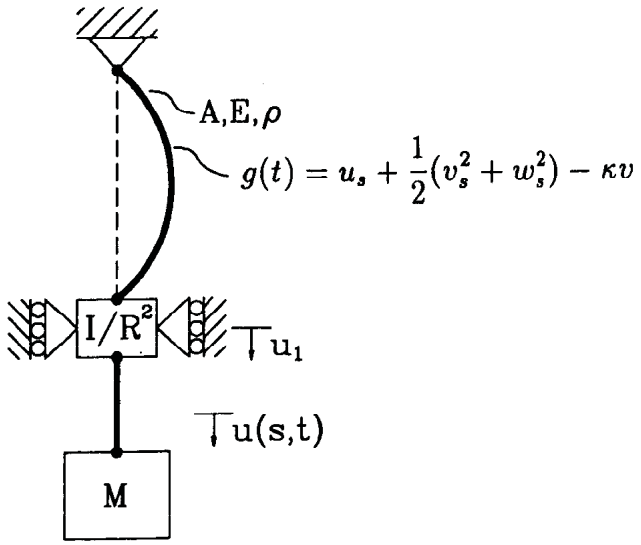

Figure 5.7: Quasi-static mine hoist model

A quasi static relationship is developed for the catenary motion by neglecting the longitudinal inertia u_{tt} in equation 5.1. As a result a constraint relationship arises which defines the quasi-static strain $g(t)$ in the catenary:

$$g(t) = u_s + \frac{1}{2}(v_s^2 + w_s^2) - \kappa v \tag{5.22}$$

Substituting this relationship into the lateral equations of motion (5.2,5.3) results in a quasi static-description for the lateral catenary motion, and the equations of motion reduce to:

$$v_{tt} + 2Vv_{s,t} = (\bar{c}^2 - V^2)v_{ss} + c^2 g(t)v_{ss} + \kappa c^2 g(t) \tag{5.23}$$

$$w_{tt} + 2Vw_{s,t} = (\bar{c}^2 - V^2)w_{ss} + c^2 g(t)w_{ss} \tag{5.24}$$

The vertical system is modelled as an unrestrained system, where the sheave inertia and the suspended mass are accounted for. When this system is attached to the catenary, it is restrained by the dynamic catenary tension, induced by the quasi-static strain $g(t)$.

$$[1+\eta\delta(0)+\zeta\delta(l_v)]u_{tt}+\mu_a u_t = c^2 u_{ss}+\mu_s u_{sst} \\ -c^2\delta(0)g(t)+F_{l_u}(t) \qquad (5.25)$$

where $u(s,t)$ represents the total longitudinal motion in the vertical rope, and $\eta=\frac{I}{mR^2}$, $\zeta=\frac{M}{m}$. $F_{l_u}(t)$ accounts for the inertial acceleration loading due to a uniform longitudinal acceleration. This is defined subsequently.

The *lateral boundary* excitation at the winder drum can be accommodated in the equations of motion via a co-ordinate transformation resulting in the forced equations of motion of the system, referenced to the base motion. This is achieved by applying co-ordinate transformations to equations (5.23,5.24,5.25) ie.:

$$\overline{v}(s,t)=v(s,t)+(1-\frac{s}{l_c})v_o(t)$$

$$\overline{w}(s,t)=w(s,t)+(1-\frac{s}{l_c})w_o(t)$$

Thus the forced equations of motion for the system are:

$$\overline{v}_{tt}+2V\overline{v}_{st}=(\overline{c}^2-V^2)\overline{v}_{ss}+c^2g(t)\overline{v}_{ss} \\ +\kappa g(t)+F_v(s,t)+F_{l_v}(s,t) \qquad (5.26)$$

$$F_v(s,t)=-(1-\frac{s}{l_c})\frac{d^2v_o}{dt^2}+2V\frac{d}{dt}(\frac{v_o}{l_c})$$

where $F_{l_v}(s,t)$ represents the additional inertial loading applied to the catenary in the in-plane direction due the radial velocity and acceleration associated with a layer change.

$$\overline{w}_{tt} + 2V\overline{w}_{s,t} = (\overline{c}^2 - V^2)\overline{w}_{ss} + c^2 g(t)\overline{w}_{ss} + F_w(s,t) \tag{5.27}$$

$$F_w(s,t) = -(1 - \frac{s}{l_c})\frac{d^2 w_o}{dt^2} + 2V\frac{d}{dt}(\frac{w_o}{l_c}) \quad ,$$

$$[1 + \eta\delta(0) + \zeta\delta(l_v]u_{tt} + \mu_a u_t = c^2 u_{ss} + \mu_b u_{ss,t} - c^2\delta(o)g(t) \tag{5.28}$$

The quasi-static strain $g(t)$ is defined by integrating equation (5.22), and applying the lateral co-ordinate transformations, and accounting for the longitudinal boundary condition at the winder drum $u_o(t)$. Thus:

$$u_1(t) = g(t)l_c + \int_o^{l_c} \kappa\overline{v} - \frac{1}{2}(\overline{v}_s^2 + \overline{w}_s^2)ds + u_o(t) \tag{5.29}$$
$$-\frac{1}{2l_c}(v_o(t)^2 + w_o(t)^2) + \frac{1}{2}\kappa l_c v_o(t)$$

where $u_1(t)$ represents the longitudinal motion at the sheave. This relationship defines the compatibility between the catenary and vertical section, as well as introducing the periodic excitation associated with the Lebus groove profile, and the transient excitation associated with a layer change, to the longitudinal system. These excitations are defined in Appendix A.

During the acceleration or deceleration phase of the winding cycle an additional inertial load is imposed on the longitudinal system. This load is applied by introducing a uniform acceleration to the entire system. Since the catenary is assumed massless, the inertial load generated due to a uniform longitudinal acceleration a_u is:

$$F_{I_u}(t) = -[1 + \eta(0) + \zeta(l_v)]a_u$$

This load is applied appropriately during the simulation. The lateral excitation due to the radial displacement and acceleration v_v and a_v at a layer change is accounted for in similar fashion, where the inertial load applied to the in-plane lateral equation is:

$$F_{I_v}(s,t) = -(1 - \frac{s}{l_c})a_v + 2V\frac{d}{dt}(\frac{v_v}{l_c})$$

The equations of motion for lateral and longitudinal motion can be discretised in the usual manner by applying the normal mode technique, or a Galerkin approximation. Since a quasi-static relationship implicitly satisfies the nonlinear relationship between the lateral and longitudinal motion in the catenary, the limitations evident in the original normal mode model are obviated. However, modal truncation is possible, and sufficient lateral and longitudinal modes would be required to simulate the system response accurately. The normal mode method is applied by assuming a spatial expansion for the lateral and longitudinal motion as:

$$u(s,t) = \sum \phi_i(s) p_i(t)$$

$$v(s,t) = \sum \overline{\Phi}_i(s) q_i(t)$$

$$w(s,t) = \sum \Phi_i(s) r_i(t)$$

where, for the out-of-plane modes, the mode shape is $\Phi_i(s) = sin(\frac{i\pi}{l_c}s)$[11] and the natural frequency is given by $\omega_i = i\pi\bar{c}/l_c$. $\phi_i(s)$ represents the longitudinal mode shapes of the unconstrained linear system, where the longitudinal natural frequencies are calculated via the frequency equation:

$$\Delta(\gamma_i) = \zeta\gamma_i^2\{cos(\gamma_i l_v) - \gamma_i\eta sin(\gamma_i l_v)\} + \gamma_i\{sin(\gamma_i l_v) + \gamma_i\eta cos(\gamma_i l_v)\}$$

where $\gamma_i = \frac{\overline{\omega}_i}{\bar{c}}$, $\overline{\omega}_i$ represents the longitudinal natural frequency, $\eta = \frac{I}{mR^2}$, $\zeta = \frac{M}{m}$ and l_v is the length of the vertical rope. The mode shape, normalised to unity at the sheave end is:

$$\phi_i(s) = cos(\gamma_i s) - \gamma_i\eta sin(\gamma_i s)$$

Since the system is unconstrained, the fundamental frequency $\overline{\omega}_1$ is trivial, reflecting the rigid body mode.

[11] Although it is usual to mass normalise the mode shape, the mode shape is normalised to unity so that the co-ordinate $r_i(t)$ reflects the maximum physical response in that mode.

Catenary curvature is accounted for in the simulation and consequently the in-plane natural frequencies may be calculated directly by applying the linear cable theory developed by Irvine and Caughey[1974], where the in-plane natural frequency for the symmetric modes is calculated from the frequency equation:

$$tan\frac{\omega_i}{2} = \frac{\omega_i}{2} - \frac{4}{\lambda^2}(\frac{\omega_i}{2})^3 \qquad i = 1,3,5\cdots$$

Where $\omega_i = \omega_i l_c/\bar{c}$, and $\lambda^2 = \frac{c^2}{(\bar{c}^2)^3}(gl_c)^2$, where ω_i represents the in-plane natural frequency of the symmetric modes.

and the mass normalised mode shape is given by:

$$\overline{\Phi}_i = \frac{2C_i}{cos(\omega_i/2)} sin\frac{\omega_i s}{2l_c} sin\frac{\omega_i}{2l_c}(s - l_c)$$

where:

$$C_i = \sqrt{\frac{\frac{1}{l_c}[cos\omega_i + 1]}{[2 + cos\omega_i - \frac{3}{\omega_i}sin\omega_i]}}$$

for $i = 1,3,5,\cdots$

To first order, the asymmetric in-plane modes induce no dynamic tension, and are identical to the out of plane modes. Thus for $i = 2,4,6\cdots$, the mass normalised mode shape is given by $\overline{\Phi}_i = \sqrt{\frac{l_c}{2}}sin(\frac{i\pi}{l_c}s)$ and the corresponding natural frequency is given by $\omega_i = i\pi\bar{c}/l_c$.

Because the catenary curvature is small, the effect of curvature on the symmetric in-plane modes is only discernible in the first in-plane mode for the descending cycle, as illustrated in figure 5.8. Since the in-plane motion is approximated via a modal expansion, for simplicity the in-plane symmetric mode shapes equivalent to those of a taut string are applied, hence $\overline{\Phi}_i = sin(\frac{i\pi}{l_c}s)$, and the natural frequencies are $\omega_i = i\pi\bar{c}/l_c$[12].

[12]Perkins[1992a] constructs a single mode in-plane model of a cable with fixed end conditions in the region of the first modal cross-over. Consequently, it is necessary to apply the correct form for the symmetric in-plane mode shape, since it is different to its corresponding out-of-plane mode shape.

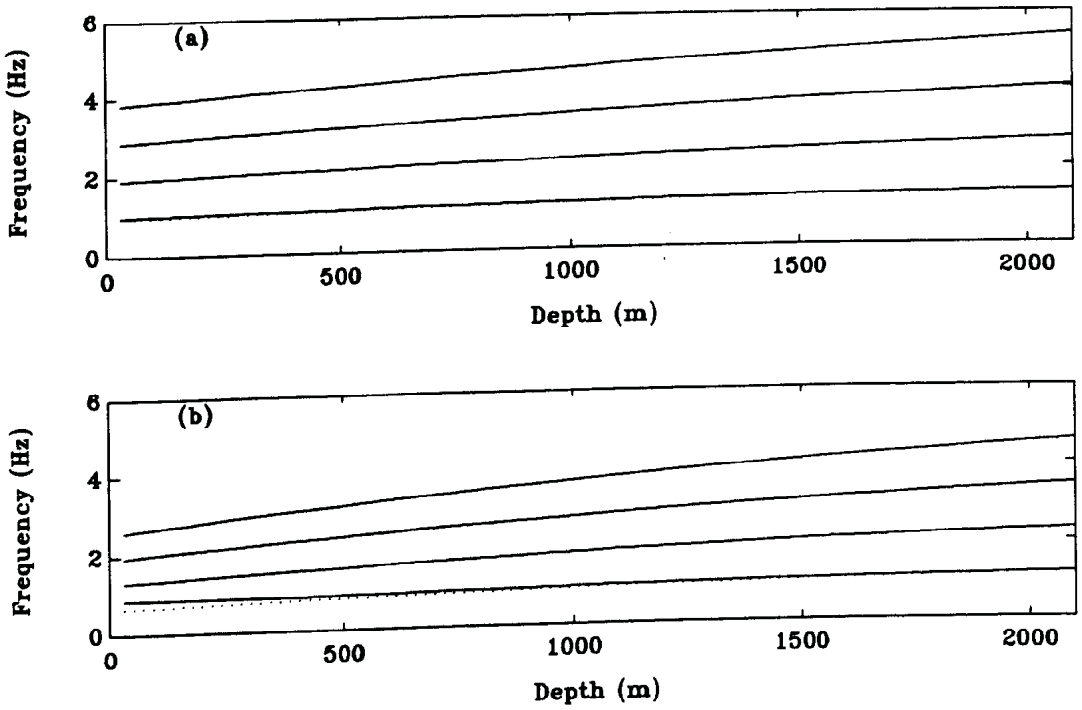

Figure 5.8: Stationary lateral natural frequencies vs shaft depth -Kloof Mine

(a) Ascending Cycle.
– - In-plane natural frequencies.

(b) Descending Cycle.
· · · · Out-of-plane natural frequencies.

On discretising the equations, a set of ordinary nonlinear differential equations result, where:

$$g(t) = \frac{1}{l_c}\sum_{i=1}^{n_{long}} p_i + \sum_{i=1}^{n_{lat}} \alpha_i q_i + \sum_{i=1}^{n_{lat}} \beta_i\{q_i^2 + r_i^2\} + F_g(t)$$

where:

$F_g(t) = -\frac{1}{l_c}\{u_o - \frac{1}{2l_c}(v_o(t)^2 + w_o(t)^2) + \frac{1}{2}\kappa l_c v_o(t)\}$
$\alpha_i = \frac{\kappa}{i\pi}\{(-1)^i - 1\}$
$\beta_i = \frac{1}{4}(\frac{i\pi}{l_c})^2$

It is noted that α_i represents the component of the quasi-static strain due to geometric realignment of the in-plane motion. As expected this component vanishes with respect to anti-symmetric modes. The discretised equations describing the longitudinal (p_i), in-plane lateral (q_i) and out-of-plane lateral (r_i) motion are presented as[13].

$$\ddot{p}_i + 2\bar{\zeta}_i\bar{\omega}_i\dot{p}_i + \bar{\omega}_i^2 p_i + c^2\{\frac{1}{l_c}p_j + \alpha_j q_j + \beta_j\{q_j^2 + r_j^2\}\} = -c^2 F_g(t) \qquad (5.30)$$

$$\ddot{q}_i + 2\zeta_i\omega_i\dot{q}_i + \mathcal{V}_{ij}\dot{q}_j + \omega_i^2\{1 + \eta_i(t)\}q_i + \zeta_i\{\frac{1}{l_c}p_j + \alpha_j q_j + \beta_j\{q_j^2 + r_j^2\}\}q_i + c^2\alpha_i\{\frac{1}{l_c}p_j + \alpha_j q_j + \beta_j\{q_j^2 + r_j^2\}\} = Q_i(t) + c^2\alpha_i F_g(t) \qquad (5.31)$$

$$\ddot{r}_i + 2\zeta_i\omega_i\dot{r}_i + \mathcal{V}_{ij}\dot{r}_j + \omega_i^2\{1 + \eta_i(t)\}r_i + \zeta_i\{\frac{1}{l_c}p_j + \alpha_j q_j + \beta_j\{q_j^2 + r_j^2\}\}q_i = R_i(t) \qquad (5.32)$$

where:

[13]In these equations the summation signs have been left out, and the subscript j refers to summation over the number of modes.

$\eta_i = (\frac{c}{\bar{c}})^2 \omega_i^2 F_g(t)$
$\zeta_i = (\frac{c}{\bar{c}})^2 \omega_i^2$
$\mathcal{V}_{i,j} = 8V\{\frac{ij}{(j^2-i^2)l_c}\} \quad i \neq j$
$\mathcal{V}_{i,j} = 0 \quad i = j$

Proportional damping has been added to the longitudinal and lateral equations of motion respectively via $\bar{\zeta}_i, \zeta_i$. The terms $P_i(t), R_i(t), Q_i(t)$ arise due to the direct excitation at the winder drum. These are evaluated as:

$$P_i(t) = \frac{1}{m_{u_{ii}}} \int_0^{l_v} \phi_i(s)\{F_u(s,t) + F_{I_u}(t)\}ds$$

$$Q_i(t) = \frac{1}{m_{v_{ii}}} \int_0^{l_c} \Phi_i(s)\{F_v(s,t) + F_{I_v}(t)\}ds$$

$$R_i(t) = \frac{1}{m_{w_{ii}}} \int_0^{l_c} \Phi_i(s) F_w(s,t)ds$$

where $m_{u_{ii}}, m_{v_{ii}}, m_{w_{ii}}$ represent the modal mass associated with the ith generalised co-ordinate.

Since α_i is zero for the antisymmetric modes, the quadratic nonlinearities introduced by the catenary curvature, and the direct excitation of the in-plane modes due to curvature coupling, vanish with respect to the anti-symmetric lateral modes. However, as with the laboratory model, quadratic coupling between the lateral and longitudinal motion is retained due to the retention of the longitudinal inertia associated with the vertical section.